Investigation of Left-Handed Behavior in Ferromagnetic Cobalt Magnetic Vortex Structure Using Spin-Wave Resonances

Madhumathi Rajaram, Amuda Rajamani, Ponsudana Muthuraj, Brinda Arumugam, and Kanimozhi Natarajan

Centre for Nonlinear Dynamics, Department of Physics, PSG College of Technology, Coimbatore 641005, India

Terahertz spintronics is an emerging field that bridges the boundary between magnetism and photonics, which make the magnetic material suitable for photonic applications. In this article, terahertz spin-wave resonances are used to investigate the effective permeability of left-handed behavior in an array of cobalt nanomagnetic vortices. The ultrafast magnetization and the toroidal moment of the cobalt nanomagnetic vortices play a major role in reducing losses in the left-handed metamaterial. The ultrafast magnetization dynamics of an array of cobalt nanomagnetic vortices are studied both analytically and numerically, and the results are used to study the variation of permeability as a function of frequency in the terahertz range.

***Index Terms*— Cobalt nanovortices, gyromagnetic equation, magnetic metamaterial, magnetic vortices, negative permeability, toroidal metamaterial.**

I. Introduction

METAMATERIALS are artificially engineered materials with anomalous nature unbound left-handed electromagnetic properties in which optical geometry plays a major role in engineering space for light [1], [2]. The metamaterial has a peculiar property of a negative refraction. According to Veselago, negative refraction can be achieved in two ways. One way to attain negative refraction is by negative refractive index. Artificially, the negative refractive index is achieved in some materials using geometrically tuned structures known as a split-ring resonator (SRR).

According to Veselago, negative refraction can also be achieved by tuning either permittivity or permeability of the material as negative. This kind of negative refraction is achieved in the case of hyperbolic metamaterials. The past two decades of research in this field revealed that most of the left-handed materials (LHMs) are fabricated only from nonmagnetic materials. In the case of hyperbolic metamaterials and SRR structures, these nonmagnetic materials are geometrically tuned to exhibit artificial magnetism which can mimic ferromagnetic behavior. The interest in artificial magnetism was driven by the fact that with optical frequency, strong natural micro magnetism was virtually nonexistent, where light–matter interactions are mediated exclusively by the electrical component of light [3].

The recent research in metamaterial revealed that the resonance frequency can alternatively rely on spin-wave resonances in natural ultrafast magnetic materials [5]. The optical magnetic response was not found in macroscopic natural magnetic materials due to the fact that the magnetization field $m(r)$ of the magnetic material cannot be reduced to the ground state by any finite deformation caused by an electromagnetic wave [4].

When the size of the magnetic material is scaled down below submicrometer and subwavelength size, then additional magnetostatic energy contributes to the total energy. As a result, the magnetization reversal happens and different eigenmode spin excitation exists in magnetic materials. This gives rise to different magnetic spin textures. Certain magnetic spin textures like a magnetic vortex and skyrmion exhibit toroidal dipole moment, and it can enhance field confinement of the electromagnetic wave by concentrating the magnetic field in a small circular region. In recent years [24], [25], the toroidal dipolar response in metamaterial has captured the imagination of researchers hoping to miniaturize and modify the properties of the existing metamaterial-based optical devices. Magnetism and left-handed behavior are the two extreme phenomena that do not seem to be compatible, and the coexistence of both cooperative effects was not foreseen in toroidal magnetic structures. In this article, an alternative route using the intrinsic magnetic resonance of an array of nanopatterned toroidal cobalt nanomagnetic vortices was used to engineer the basic dispersion relation of waves to obtain negative refraction. Here, the transient magnetization dynamics are calculated for excitation with terahertz (THz) external electromagnetic field pulses.

The interaction of the electromagnetic wave with cobalt nanomagnetic vortices was studied both analytically and numerically. Since the nanomagnetic dynamics involve ultrafast magnetization dynamics, the inertial Landau–Lifshitz–Gilbert (LLG) equation was used to study the dynamics of magnetic vortices. From the magnetization values obtained from numerical results, Schloemann model was used to theoretically derive the permeability values as a function of frequency. Due to the natural toroidal response of magnetic vortices, the magnetic vortices with the same geometrical parameters obtained using mumax[3] were numerically simulated using CST microwave studio, and the corresponding left-handed response was analyzed.

Manuscript received October 31, 2019; revised February 27, 2020; accepted March 6, 2020. Date of publication March 10, 2020; date of current version July 20, 2020. Corresponding author: A. Rajamani (e-mail: amuacademics@gmail.com).

Color versions of one or more of the figures in this article are available online at http://ieeexplore.ieee.org.

Digital Object Identifier 10.1109/TMAG.2020.2979791

II. Gyromagnetic Equation

The gyromagnetic equation is used to represent the frequency at which the magnetic system will absorb energy, and it depends on Larmor precession. With the burgeoning developments in the nano optical ferromagnetic devices, the interest in myriad types of magnetic materials is growing rapidly. The myriad type of magnetic materials owes their unique utility in optical technology due to the phenomenon of ferromagnetic resonance (FMR). The magnetic system under the influence of the external dc magnetic field will undergo precession. The angular frequency of this precession is given by the product of $\gamma 4\pi \overrightarrow{M}$. If a small electromagnetic field present in addition to the dc field, and if the frequency of the electromagnetic field coincides with the precessional frequency, the amplitude of the spin precession will go indefinitely. This phenomenon is known as FMR.

Since the nanomagnetic material involves ultrafast magnetization dynamics, the inertial LLG equation was employed to find the analytical solution of gyromagnetic motion. The kinetic equation which takes into account the complete dynamical motion of magnetization vector was given by the nonlinear LLG equation

$$\frac{d\overrightarrow{M}}{dt} = \gamma\, \overrightarrow{M} X \left[\overrightarrow{H}^{\text{eff}} - \eta\left(\frac{d\overrightarrow{M}}{dt}\right)\right]$$

where $\overrightarrow{M}$ is the magnetization and $\overrightarrow{H}^{\text{eff}}$ is the effective magnetic field, γ is the gyromagnetic ratio, and $\eta = (\alpha/\boldsymbol{M}_s)$, where α is the Gilbert damping factor, and $\boldsymbol{M}_s$ is the saturation magnetization. This kinetic LLG equation fits only for noninertial frames that do not involve acceleration. The soundness of this LLG equation is adequate only to large time scales and a low-frequency region and for higher relaxation time [6]. For the ultrafast magnetization dynamics and high frequencies, inertia plays a dynamic role. For ultrafast magnetization dynamics, the LLG equation was augmented by an additional term that describes the drift in the magnetization dynamics. The LLG equation with this additional supplementary inertial term is called inertial LLG (ILLG) equation. The ILLG equation reads [28]

$$\frac{d\overrightarrow{M}}{dt} = \gamma\, \overrightarrow{M} X \left[\overrightarrow{H}^{\text{eff}} - \eta\left(\frac{d\overrightarrow{M}}{dt} + \tau\frac{d^2\overrightarrow{M}}{dt^2}\right)\right]. \tag{1}$$

The magnetic field is applied along the z-direction and the circularly polarized irradiation field is applied in the XY plane, (1) in terms of its components can be written as

$$\frac{dm_x}{dt} = \gamma\left(m_y H_z - m_z H_y\right) - \gamma\,\eta\left(m_y\frac{dm_z}{dt} - m_z\frac{dm_y}{dt}\right) - \gamma\,\eta\tau\left(m_y\frac{d^2m_z}{dt^2} - m_z\frac{d^2m_y}{dt^2}\right) \tag{2}$$

$$\frac{dm_y}{dt} = \gamma\left(m_z H_x - m_x H_z\right) - \gamma\,\eta\left(m_z\frac{dm_x}{dt} - m_x\frac{dm_z}{dt}\right) - \gamma\,\eta\tau\left(m_z\frac{d^2m_x}{dt^2} - m_x\frac{d^2m_z}{dt^2}\right) \tag{3}$$

$$\frac{dm_z}{dt} = \gamma\left(m_z H_x - m_x H_z\right) - \gamma\,\eta\left(m_x\frac{dm_y}{dt} - m_y\frac{dm_x}{dt}\right) - \gamma\,\eta\tau\left(m_x\frac{d^2m_y}{dt^2} - m_y\frac{d^2m_x}{dt^2}\right). \tag{4}$$

Since the magnetic field is applied along the z-direction, the variation of the magnetization along the z-direction will be constant $(dm_z/dt) = 0$, so now (2) and (3) become

$$\frac{dm_x}{dt} = \gamma\left(m_y H_z - m_z H_y\right) + \gamma\,\eta\left(m_z\frac{dm_y}{dt}\right) + \gamma\,\eta\tau\left(m_z\frac{d^2m_y}{dt^2}\right) \tag{5}$$

$$\frac{dm_y}{dt} = \gamma\left(m_z H_x - m_x H_z\right) - \gamma\,\eta\left(m_z\frac{dm_x}{dt}\right) - \gamma\,\eta\tau\left(m_z\frac{d^2m_x}{dt^2}\right). \tag{6}$$

Differentiating (5) and (6) reads as

$$\frac{d^2m_x}{dt^2} = \gamma\left(H_z\frac{dm_y}{dt} - m_z\frac{dH_y}{dt}\right) + \gamma\,\eta\left(m_z\frac{d^2m_y}{dt^2}\right) + \gamma\,\eta\tau\left(m_z\frac{d^3m_y}{dt^3}\right) \tag{7}$$

$$\frac{d^2m_y}{dt^2} = \gamma\left(m_z\frac{dH_x}{dt} - H_z\frac{dm_x}{dt}\right) - \gamma\,\eta\left(m_z\frac{d^2m_x}{dt^2}\right) - \gamma\,\eta\tau\left(m_z\frac{d^3m_x}{dt^3}\right). \tag{8}$$

Differentiating (8) reads as

$$\frac{d^3m_y}{dt^3} = \gamma\left(m_z\frac{d^2H_x}{dt^2} - H_z\frac{d^2m_x}{dt^2}\right) - \gamma\,\eta\left(m_z\frac{d^3m_x}{dt^3}\right) - \gamma\,\eta\tau\left(m_z\frac{d^4m_x}{dt^4}\right). \tag{9}$$

On substituting (6), (8) and (9) in (7), (7) becomes

$$\gamma^2\eta^2\tau^2m_z^2\frac{d^4m_x}{dt^4} + 2\gamma^2\eta^2m_z^2\tau\frac{d^3m_x}{dt^3} + \left(2\gamma^2\eta\tau m_z H_z + \gamma^2\eta^2m_z^2 + 1\right)\frac{d^2m_x}{dt^2} + 2\gamma^2H_z\eta m_z\frac{dm_x}{dt} + \gamma^2H_z^2m_x = \gamma^2\eta\tau m_z^2\frac{d^2H_x}{dt^2} + \gamma^2\eta m_z^2\frac{dH_x}{dt} - \gamma\,H_z m_z\frac{dH_y}{dt} + \gamma^2m_z H_z. \tag{10}$$

Similarly, the y-component equation becomes

$$\gamma^2\eta^2\tau^2m_z^2\frac{d^4m_y}{dt^4} + 2\gamma^2\eta^2m_z^2\tau\frac{d^3m_y}{dt^3} + \left(2\gamma^2\eta\tau m_z H_z + \gamma^2\eta^2m_z^2 + 1\right)\frac{d^2m_y}{dt^2} + 2\gamma^2H_z\eta m_z\frac{dm_y}{dt} + \gamma^2H_z^2m_y = \gamma^2\eta\tau m_z^2\frac{d^2H_y}{dt^2} - \gamma^2\eta m_z^2\frac{dH_x}{dt} + \gamma^2\eta m_z^2\frac{dH_y}{dt} + \gamma^2m_z H_z H_x. \tag{11}$$

Equation (11) represents the second derivative of acceleration which is jounce. The components of THz circularly polarized irradiation field are $H_x = H\cos\omega t$ and $H_y = H\sin\omega t$. Using the trignometric synthesis formula, H_x and H_y components can

be written as a single term and the magnetization component equation in terms of frequency can be read as

$$\gamma^2\eta^2\tau^2 m_z^2\frac{d^4m_x}{dt^4}+2\gamma^2\eta^2 m_z^2\tau\frac{d^3m_x}{dt^3}+\left(2\gamma\omega_0\eta\tau m_z+\gamma^2\eta^2 m_z^2+1\right)\frac{d^2m_x}{dt^2}+2\gamma\eta\omega_0 m_z\frac{dm_x}{dt}+\omega_0^2 m_x=\gamma m_z\sqrt{\left(\gamma m_z\eta\tau\omega^2+\omega-\omega_o\right)^2+(\eta\omega)^2}H\cos\omega t \tag{12}$$

where $\omega_0=\gamma H_z$ is the frequency corresponding to the external magnetic field. Both right-hand sides of (12) represent the periodic force term of the irradiation field. The particular solution of the differential equation of the form

$$m_x=C\cos(\omega t+\varphi) \tag{13}$$

where

$$C=\frac{\gamma H m_z\sqrt{\left(\gamma m_z\eta\tau\omega^2+\omega-\omega_0\right)^2+(\eta\omega)^2}}{\sqrt{A^2+B^2}}. \tag{14}$$

Equation (13) represents the equilibrium state of the forced oscillation. This equation resembles the particular solution of a simple harmonic oscillator with amplitude C and phase φ. The resonance frequency of the oscillator is given by $\omega=(\varphi/t)$. This shows that the FMR frequency depends on the variation of phase. From (15), as shown at the bottom of this page, we can infer that the phase depends on the damping factor and the relaxation time. So with the proper value of relaxation time and damping factor for ultrafast magnetization dynamics, the frequency of the above system can be tuned.

A. Numerical Micromagnetics

With rapidly increasing developments in nanoscience and technology, the interest in the myriad type of magnetic nanoparticle is growing rapidly due to the quantum confinement of electrons. In this article, Using Mumax[3] we numerically simulate the evolution of spin structures in cobalt nanodisc on the platinum thin-film substrate. Cobalt nanoparticles have impressive magnetic properties due to its high magnetocrystalline anisotropy and high coercive force compared to other myriad magnetic materials and permalloy [7]. The system under study consists of an array of cobalt nanodisc on a platinum substrate. As shown in Fig. 1, a static magnetic field, $\overrightarrow{H_z}$ is applied along the z-axis and an external electromagnetic field $\overrightarrow{h}\,e^{j\omega t}$ was applied along the *XY* plane. The spin angular momentum precesses around the resultant field vector direction $\overrightarrow{H_z}+\overrightarrow{h}\,e^{j\omega t}$ and it makes an angle θ with the z-axis.

In natural magnetic materials, by scaling the system down to the nanometer scale, the spin of the nanostructure twist, move, deform, and form different unique magnetic spin textures. Some of the unique spin texture of the nanomagnetic materials leads to enthralling phenomena that show magnetic toroidal behavior above THz frequency due to the topologically protected quantum state and delocalized magnetic moments [8]. The macroscopic ferromagnetic material exhibits long-range parallel spin configuration. When the length scale in the nanomagnetism approach critical exchange length, the stochastic nature of the ferromagnetic material was out of the box and magnetization reversal starts to occur and form different spin textures [9].

Magnetic vortex is one of the ground state magnetic quasi-particle spin textures that have potential applications in magnonic and spintronic devices. They are the point-like region of reversed magnetization, surrounded by a whirling twist of spins. They are very stable and easily manipulated by spin-polarized currents that consume little power. The magnetic vortex structure originates from many interactions like exchange interaction, magnetocrystalline anisotropy, demagnetization, and DMI. The system energy function was studied by the following energy equation:

$$\varepsilon(\overrightarrow{m})=A\sum_{\alpha=x,y,z}\left(\vec{\nabla}m\alpha\right)^2-k_u m_z^2-\frac{M_s}{3}\mu_0\vec{m}\cdot\vec{H}_d-M_s\vec{m}\cdot(\vec{H}_z+\overrightarrow{h}\,e^{j\omega t})$$

where the first represents exchange energy with stiffness constant A, the second term represents uniaxial anisotropy energy with an anisotropy constant k_u, and the successive terms represent magnetostatic energy and Zeeman energy. Zeeman term not only includes the external magnetic field but also includes the oscillatory electromagnetic field.

Simulations were carried with standard parameters of Cobalt, saturation magnetization $M_s=1.424\text{e}+6\ \text{Am}^{-1}$, exchange stiffness $A=2.5\text{e-}11\text{Jm}^{-1}$, uniaxial anisotropy constant $k_u=4\text{e}+5\ \text{erg cm}^{-3}$, damping constant $\alpha=0.01$, and the relaxation time $\tau=3$ fs. The critical radius below which a particle magnetostatic energy dominates and form a single domain is given by $R_c=9(\sqrt{Ak_u}/\mu_0 Ms^2)$. Using the above expression, typical values of the critical radius of Cobalt to form a single domain for ultrafast magnetization were found to be about 35 nm [7]. The exchange length was given by

$$A=\frac{\gamma H m_z\sqrt{\left(\gamma m_z\eta\tau\omega^2+\omega-\omega_0\right)^2+(\eta\omega)^2}\left(\gamma^2\eta^2\tau^2 m_z^2\omega^4-2\gamma\omega_0\eta\tau m_z\omega^2-\gamma^2\eta^2 m_z^2\omega^2-\omega^2+\omega_0^2\right)}{(2\gamma\eta\omega_0\omega m_z-2\gamma\eta\omega_0\omega m_z)^2+\left(\gamma^2\eta^2\tau^2 m_z^2\omega^4-2\gamma\omega_0\eta\tau m_z\omega^2-\gamma^2\eta^2 m_z^2\omega^2-\omega^2+\omega_0^2\right)}$$

$$B=\frac{\gamma H m_z\sqrt{\left(\gamma m_z\eta\tau\omega^2+\omega-\omega_0\right)^2+(\eta\omega)^2}\left(2\gamma^2\eta^2 m_z^2\omega^3\tau-2\gamma\omega_0 m_z\omega\right)}{(2\gamma\eta\omega_0\omega m_z-2\gamma\eta\omega_0\omega m_z)^2+\left(\gamma^2\eta^2\tau^2 m_z^2\omega^4-2\gamma\omega_0\eta\tau m_z\omega^2-\gamma^2\eta^2 m_z^2\omega^2-\omega^2+\omega_0^2\right)^2}$$

$$\varphi=\tan^{-1}\left(-\frac{\left(2\gamma^2\eta^2 m_z^2\omega^3\tau-2\gamma\omega_0 m_z\omega\right)}{\left(\gamma^2\eta^2\tau^2 m_z^2\omega^4-2\gamma\omega_0\eta\tau m_z\omega^2-\gamma^2\eta^2 m_z^2\omega^2-\omega^2+\omega_0^2\right)}\right) \tag{15}$$

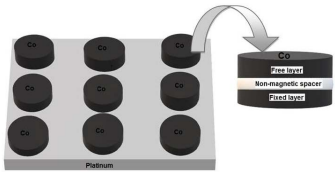

Fig. 1. Illustration of the model of an array of cobalt spin-valve pillars on a platinum substrate.

$l_{ex} = \sqrt{(A/2\pi Ms^2)}$. The relation between critical the radius and exchange length is $R_c = 2.6\ l_{ex}$.

Taking critical radius and exchange length into consideration, micromagnetic simulations have been performed on an array of Co/Pt alloy having a lateral size of 50 nm and thickness of 3 nm. Fig. 1 illustrates the model of an array of Cobalt spin-valve pillars on a platinum substrate. Each cobalt nanodisc was made to consist of a fixed layer, nonmagnetic spacer, and the free layer. In general, both short-range exchange and long-range magnetostatic interactions contribute to eigenfrequencies of the collective spin excitation.

B. Nucleation of the Magnetic Vortex

The spatial and temporal variation of the reversal of magnetization vector in the circular Cobalt nanodisc was analyzed as a function of the applied magnetic field for the constant oscillatory electromagnetic field and a sequence of typical domain structure at the magnetic field ranging from 120 to −120 mT with hysteresis loop variation are shown in Fig. 2(a)–(e). The external magnetic field was applied along z-direction and the magnetization changes were observed along the XY plane. The external magnetic field produces a magnetoelectric effect in which it induces an energy difference between states with different orientations of the order parameter. This field is used to switch the domain states with the lowest energy orientation.

The critical radius of the cobalt nanodisc induces local strain in the film which introduces strong pinning sites for the magnetization. The shape of the element, uniaxial anisotropy, and magnetostatic energy mainly contribute to the magnetic states and switching behavior. In circular nanodisc, the magnetization will predominantly follow the circumference to minimize the stray field leading to flux closure vortex state with an anticlockwise circulation of magnetization.

Prior to the nucleation of the magnetic vortices, as a thumb rule, at saturation, the nanodisc predominantly showed single domain uniform magnetization state, i.e., the magnetization vector of an array of cobalt nanodisc undergo coherent rotation and align along the equilibrium direction, so that $\vec{M} = Ms\vec{Z}$. The magnetic field corresponding to the saturation magnetization was 100 mT [Fig. 2(a)].

After saturation, the external magnetic field was reduced in steps of 1 mT down to −100 mT. When the field was reduced to −20 mT, the magnetization follows the circumference of the nanodisc and enters into the magnetic vortex state [Fig. 2(b)]. At each field step time, the evolution of the magnetization vector was calculated with mumax[3].

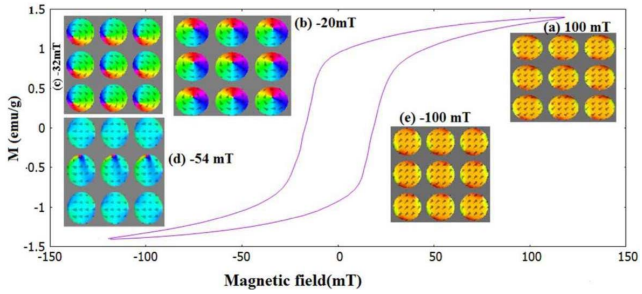

Fig. 2. Hysteresis loop of Co/Pt alloy with the corresponding evolution of spin for varying magnetic fields ranging from 100 to −100 mT. (a) Saturation magnetization with a corresponding magnetic field of 100 mT. (b) Magnetic vortex state with a corresponding magnetic field of −20 mT. (c) Core-shifted magnetic vortex corresponding to the magnetic field of −32 mT. (d) Parallel magnetization state with a corresponding magnetic field of −54 mT. (e) Reverse saturation magnetization with a corresponding magnetic field of −100 mT.

The nucleation of the magnetic vortex was accompanied by the following two transition states. The first transition state occurs with parallel magnetization [Fig. 3(a)] to decrease the dipolar energy compared to the disk in saturation. The magnetic field associated with this transition state is 78 mT. It was easy to switch from uniform magnetization to parallel magnetization state because this occurs soon after saturation and before remanence.

In the second transition state, parallel magnetization enters into the buckling state [Fig. 3(b)]. When the external magnetic field was about −10 mT, the angle between the spins increased spontaneously, leading to buckling state. This transition state exists for the magnetic field ranging from −10 to −20 mT. The buckling state consists of two vortex cores and two domain walls around which the magnetization was curling in opposite directions.

Upon a further decrease in the plane field, the vortex core starts to move toward each other. This decreases the net magnetization along field direction and the magnetization annihilates and forms vortex with a single core [Fig. 3(c)]. A magnetic vortex consists of out-of-plane magnetizations at its core region and in-plane curling around the vortex core. Upon a further decrease in the magnetic field, the magnetic vortex core shifted for the magnetic field value of −32 mT [Fig. 2(c)]. This occurs due to the small gyration of the magnetic vortex induced by the external magnetic field. When the magnetic field value was further decreased, the vortex core polarization toggles back and again enter into a parallel magnetization state for the magnetic field value of −54 mT [Fig. 2(d)]. Further decrease in a magnetic field leads to the reverse saturation state for the magnetic field of −100 mT [Fig. 2(e)]. The transition time involved in all the transitions was in femtoseconds and the system undergoes ultrafast magnetization transition.

C. Determination of Permeability of Magnetic Vortices-Schloemann Model

The operating frequencies of the metamaterial devices are becoming increasingly varied with more diversity of functionality coming from a variety of devices, working at

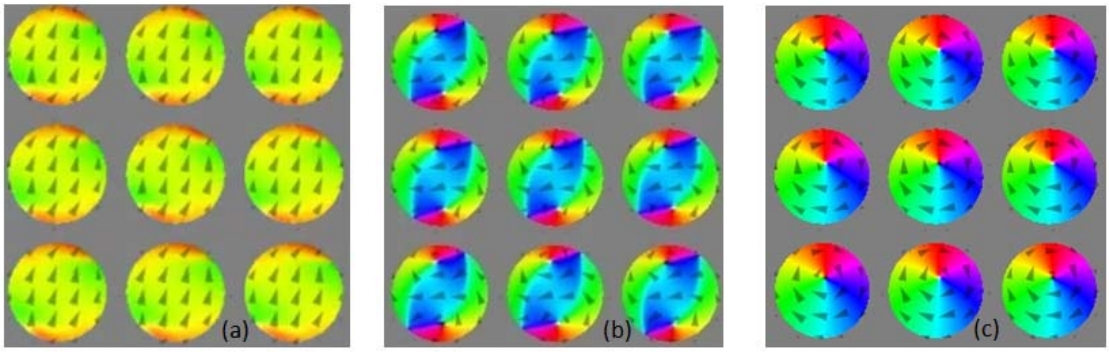

Fig. 3. Nucleation of magnetic vortices. (a) Parallel magnetization state. (b) Buckling state. (c) Magnetic vortex state.

different frequency levels to serve a variety of heterogeneous functions. With the burgeoning development in the ultrafast magnetism, the sub-picoseconds and femtoseconds demagnetization dynamics in magnetic nanoparticle stimulated by THz radiation have been observed [10], [11]. The ultrafast magnetization requires a stimulus that is capable of controlling the magnetization more rapidly. The THz radiation has the capability to overcome the GMR speed limits in ferromagnets which has femtosecond magnetization switching variation. The rate of change of time for the observed array of cobalt nanodisc was found to be in a femtosecond. Therefore, THz radiation was used as a stimulus to study the resonance behavior of cobalt nanoparticles. The key magnetic properties for electromagnetic passive components are permeability and frequency stability. Designing the ferromagnetic optical devices requires the knowledge of magnetic permeability.

According to the Global model, the permeability was assumed to be based on the two factors: (i) domain wall rotation and (ii) spin rotation[12]. At low frequency, the domain wall motion dominates more and contribute to the permeability. At high frequencies, the spin rotational gyromagnetic torque dominates and contributes to the magnetic permeability. In the present system, the domain wall is single domain wall and the spin dynamics take place in femtoseconds so high-frequency radiation is considered for the study of magnetic vortices. Spin gyrotropic motion mainly contributes to the permeability tensor. The resonance behavior of the partially magnetized state occurs when the frequency was found to be below the resonance frequency of saturation magnetization $\omega = \gamma 4\pi M_s$ [13]. The frequency corresponding to the saturation magnetization for the array of cobalt nanodisc was found to be 19.456 THz. Therefore, the resonance behavior of Cobalt nanodisc was studied below 19 THz.

To determine the permeability tensor of an array of magnetic vortices, Schloemann model was considered. The Schloemann method is used to determine the permeability of the magnetic system, whose magnetization value cycled between different states in the hysteresis loop [22]. Initially in this model, saturation magnetization was assumed. During the demagnetization process, the system tends to have a local permeability tensor. When the THz optical radiation was applied to the partially magnetized cobalt vortices, due to the opto-magnetic interaction the Zeeman torque $\tau = \overrightarrow{S} X \overrightarrow{B}$ was induced by the magnetic oscillating magnetic field component $\overrightarrow{B}$ of the THz pulse.

As a result, the magnetization will be either parallel or perpendicular to the z-axis due to resonantly excited vortex gyrotropic mode. The vortices can be considered as a cylinder whose axis is aligned along the z-axis. Since there are no magnetization changes along the z-direction, the permeability changes along that direction will be unity. In this theory, the variation of dc magnetic moment with the dc bias field is neglected by way of approximation ("constant-Mz" model). In the present case, the magnetization dynamics is studied in cobalt spin-valve pillars. The spin-valve pillar is in the form of a squat circular cylinder. The cylinder is a special case of an oblate spheroid. For a squat cylinder, the longitudinal demagnetizing factor N_l equals 1 and the transverse demagnetizing factor N_t equals zero [14]. For a fully demagnetized sample of cylindrical shape, the optical permeability is expected to be a function of the internal magnetic field H_{int}, demagnetizing factor, and the applied external magnetic field H_{ext}, and its relation is given by

$$H_{\text{int}} = H_{\text{ext}} - 4\pi MN$$

where M is the dc magnetization and N is the demagnetizing factor. The relation between the irradiation field and magnetization is

$$\overrightarrow{M} = \chi_{\text{ext}} h.$$

The external susceptibility is related to the internal susceptibility by

$$\chi_{\text{ext}} = \frac{\chi_{\text{int}}}{1 + (N_t - N_l)\chi_{\text{int}}}.$$

For circular polarization of light, the internal susceptibility is given by

$$\chi_{\text{int}} = \chi_{\pm} = \frac{\omega_m}{\omega_H + j\alpha\omega \mp \omega}$$

where $\omega_m = \gamma 4\pi M_s$ and $\omega_H = \gamma 4\pi M$.

For positive circular polarization of light, the external susceptibility in terms of internal susceptibility is given by

$$\chi_{\text{ext}+} = \frac{\omega_m}{\omega_H + (N_t - N_l)\omega_m - \omega}$$
$$\chi_{\text{ext}-} = \frac{\omega_m}{\omega_H + (N_t - N_l)\omega_m + \omega}.$$

The magnetic permeability tensor response to an alternating external magnetic field was expressed by

$$\mu_e = \begin{pmatrix} \mu_e & -jk_e & 0 \\ jK_e & \mu_e & 0 \\ 0 & 0 & \mu_{e_z} \end{pmatrix}.$$

Since the magnetic field is applied along the z-direction, the magnetization variation along the z-direction becomes unity. Now, the magnetic permeability was given by

$$\mu_e = \begin{pmatrix} \mu_e & -jk_e & 0 \\ jK_e & \mu_e & 0 \\ 0 & 0 & 1 \end{pmatrix}.$$

The tensor components μ_e and k_e represent the perpendicular and parallel permeability components. In terms of susceptibility, the two equations can be written as

$$\mu_e = 1 + \frac{(\chi_+ + \chi_-)}{2}, \qquad k_e = -\left(\frac{(\chi_+ - \chi_-)}{2}\right).$$

The expression for μ_e and k_e was given by

$$\mu_e = 1 + \frac{MM_s - M_s^2}{(M + (N_t - N_l)M_s)^2 - \left(\frac{\omega}{\gamma 4\pi}\right)^2}$$

$$k_e = -\frac{\frac{\omega M_s}{\gamma 2\pi}}{(M + (N_t - N_l)M_s)^2 - \left(\frac{\omega}{\gamma 4\pi}\right)^2}.$$

Since for squat cylindrical spin-valve pillar, $N_t = 0$ and $N_l = 1$. The expression for permeability μ_e and k_e becomes

$$\mu_e = 1 + \frac{MM_s - M_s^2}{(M - M_s)^2 - \left(\frac{\omega}{\gamma 4\pi}\right)^2}$$

$$k_e = -\frac{\frac{\omega M_s}{\gamma 2\pi}}{(M - N_l M_s)^2 - \left(\frac{\omega}{\gamma 4\pi}\right)^2}.$$

Here, M is the magnetization corresponding to the magnetic field that exists inside the domain in the direction of magnetization, γ is the gyromagnetic ratio, ω is the gyromagnetic resonance frequency, and M_s is the saturation magnetization. In the present system, magnetic vortices were formed in the free layer of the cylindrical spin-valve pillar. Since the magnetization along the z-direction was unity, the spin-valve pillar can be considered as cylindrically symmetric. According to Rado's work, for the cylindrical symmetric system, μ_e can be considered as a function of net magnetization at which k_e vanishes [15]. So for the present system, the off-diagonal components of the permeability tensor vanish. Now, the permeability tensor can be represented as

$$\mu_e = \begin{pmatrix} \mu_{\text{eff}} & 0 & 0 \\ 0 & \mu_{\text{eff}} & 0 \\ 0 & 0 & 1 \end{pmatrix}.$$

Then, the effective permeability becomes

$$\mu_{\text{eff}} = \sqrt{\frac{\frac{\omega^2}{\gamma^2} - (M + 4\pi M_s)^2}{\frac{\omega^2}{\gamma^2} - M^2}}.$$

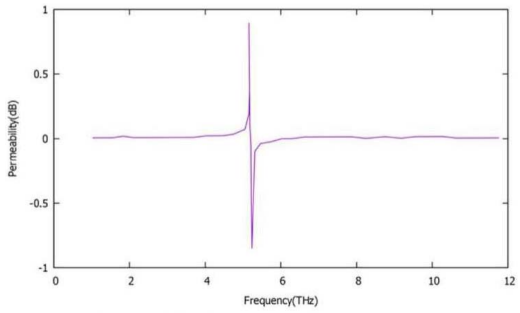

Fig. 4. Determination of permeability of magnetic vortices using the Schloemann model and the resonance frequency was found to be around 5.23 THz.

This permeability is real when $(\omega/\gamma) > M + 4\pi M_s$ and imaginary when $(\omega/\gamma) < M + 4\pi M_s$.

Since the magnetization was unity along the z-axis. By making the spatial average of the three diagonal elements of the local permeability tensor, the average effective permeability was

$$\mu_{\text{eff}} = \frac{2}{3}\sqrt{\frac{\left(\frac{\omega}{\gamma}\right)^2 - (M + 4\pi M_s)^2}{\left(\frac{\omega}{\gamma}\right)^2 - M^2}} + \frac{1}{3}.$$

The above equation in terms of frequency can be expressed as

$$\mu_e = \frac{2}{3}\sqrt{\frac{\omega^2 - (\omega_o + \omega_m)^2}{\omega^2 - \omega_o^2}} + \frac{1}{3}$$

where ω is the microwave signal frequency, ω_m is the frequency corresponding to the saturation magnetization ($\omega_m = \gamma M_s$), and ω_o gyromagnetic resonance frequency ($\omega_o = \gamma M$).

With the magnetization value obtained from numerical simulation and using the Schloemann model, the permeability was calculated for the cobalt vortices. For the above-described system, with the known values of saturation magnetization and the magnetization variation corresponding to the applied external magnetic field and the irradiation field, the permeability was calculated as a function of frequency and the corresponding graph was shown in Fig. 4.

From the permeability graph, it was found that the permeability value was negative between 5.20 and 5.93 THz, and the corresponding spin-wave resonances were found around 5.23 THz. Since the permeability was found to be negative between 5.2 and 5.93 THz, we infer that the system under study exhibit negative refraction between 5.20 and 5.93 THz and possess the property of left-handed metamaterial.

III. Toroidal Dipolar Response of the Magnetic Vortex

Electromagnetic potentials generated by the distribution of charges and currents were incomplete until Zeldovich in 1957 first proposed toroidal multipoles [16]. The order of vortices induced by an external magnetic field exhibits toroidization [17]. The magnetic vortices are characterized by the chiral edge states. Because of chiral edge states, the series of circulating magnetic currents occur. These currents may

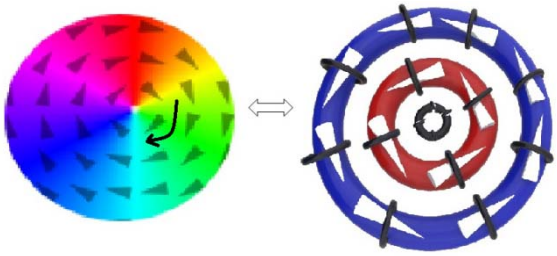

Fig. 5. Illustrates the model of the magnetic vortex as concentric toroidal rings.

produce electric fields perpendicular to it and, hence, electric fluxes through the loop. This gives rise to toroidal dipole moment in a magnetic vortex structure [17].

The toroid was formed by a set of magnetic dipoles and arranged head-to-tail along a loop. The magnetic vortex can be visualized as a series of concentric toroids with the head-to-tail alignment of magnetic dipoles and poloidal currents flowing along its meridian. Toroidal dipole moment was characterized by the change in the spatial inversion and time-reversal symmetry [18]. The existence of both spatial inversion and time-reversal was observed in magnetic vortices. As observed in Fig. 5, the counterclockwise rotation of the magnetic vortices will change into clockwise rotation under spatial inversion, and time reversal will invert electric current and spin.

In this article, an array of cobalt magnetic vortex was successfully simulated using mumax[3] software. Despite the rich magnetic structure of cobalt nanoparticle, this exhibits sole static electromagnetic toroidal dipolar response due to the formation of magnetic vortices. In the array of magnetic vortices, the order of localized spin breaks spatial inversion and time-reversal symmetry and exhibits toroidization due to delocalized magnetic moments [19]. The resulting toroidal moment was given by

$$\vec{T} = \left(g\frac{\mu_B}{2}\right)\sum_{\alpha}\vec{r_\alpha} X \vec{S_\alpha}.$$

For the system with non-vanishing magnetic moments, the toroidal moments depends on the choice of the origin of the core. If it is shifted from $\vec{r}$ to $\vec{r'} = \vec{r} + \vec{R_0}$, the toroidal moment can be expressed as $\vec{T'} = \vec{T} + (g(\mu_B/2))\sum_\alpha \vec{R_0} X \vec{S_\alpha}$. The toroid was formed by a set of magnetic dipoles m arranged head-to-tail along a loop. As shown in Fig. 5, the magnetic vortex was considered to be made up of series of a concentric toroid with the head-to-tail alignment of magnetic dipoles and poloidal currents flowing along its meridian. The electromagnetic response of the magnetic vortex was directly related to the resonant excitation of the toroidal dipole.

Up until now, an important disadvantage in making out toroidal metamaterial is the complicated design of the toroidal metal molecules capable of maintaining strong toroidal excitations [20]. However, in the magnetic vortex structure, the strong toroidal excitations are naturally well maintained. So that, it is naturally suitable for toroidal metamaterials. The important limitation of nonmagnetic metamaterials is the

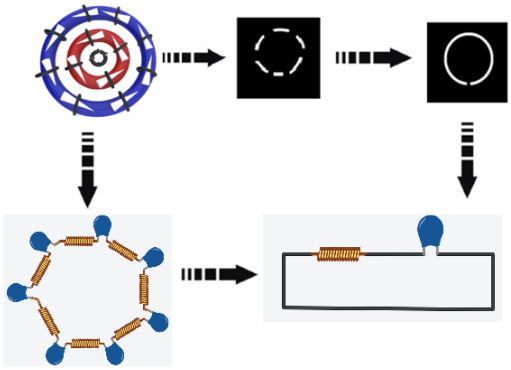

Fig. 6. Equivalent *LC* circuit of the toroidal magnetic vortex.

Joule losses at a higher frequency which is compensated by using subwavelength magnetic materials. Toroidal currents are generated by the magnetic vortex and these charge-current configurations generate vector potential fields in the absence of radiated electromagnetic waves [21]. If the electromagnetic wave interacts with this vector potential field which is in resonance with the electromagnetic wave, then it will be well confined by the magnetic vortices.

IV. Magnetic Vortex—Equivalent LC Circuit

Usually, the SRR structure consists of inductance with a small capacitive gap at the center of one arm of the circular resonator and exhibits resonance mode at a particular frequency. In the quasi-static region, the optical response of the toroidal magnetic vortex structure can be suitably modularized by considering the nano elements by an equivalent resonance circuit. The toroidal resonance in the magnetic vortices is caused by an oscillation of charges flowing in radial directions between the inner and outer rims of the toroid. The circulating current around the upper and lower parts of the toroid flows with 180° out of phase with each other [22]. This induces effective inductance L_{eff} in the toroid, and it acts like a doughnut-shaped solenoid. Hence, as shown in Fig. 6 for the light–matter interaction of the magnetic vortices, the subwavelength toroidal nanorings can be seen as the resonant interconnection of optical nanoinductors (head-to-tail arrangement of circulating magnetic field) and nanocapacitors (accumulated charges). This interpretation indicates that magnetic vortices can be considered as an optical equivalent of SRR.

Since the magnetic field around the circular toroid is zero, it will not produce an inductive effect in the nearby coil. So, each ring of the toroid can be considered to be made up of alternative inductance and capacitance in series, and all the three rings are isolated from each other due to the circular toroidal moment. In this article, the optical response of the magnetic vortices and the resonance frequency was tuned by considering concentric toroids of different radius.

V. Individual Structure Simulation

It was shown that a toroidal metamaterial an array of toroidal solenoids shows a significant electromagnetic response and has intriguing electromagnetic properties [22]–[24]. Due to the unique property of concentrating

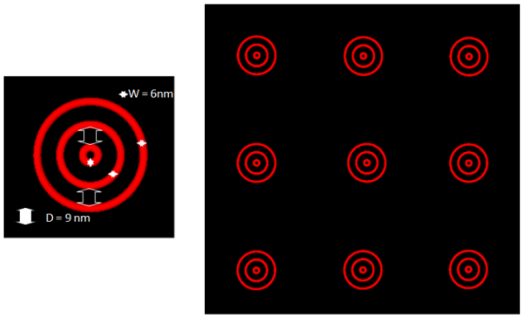

Fig. 7. Unit cell and full structure of the proposed metamaterial.

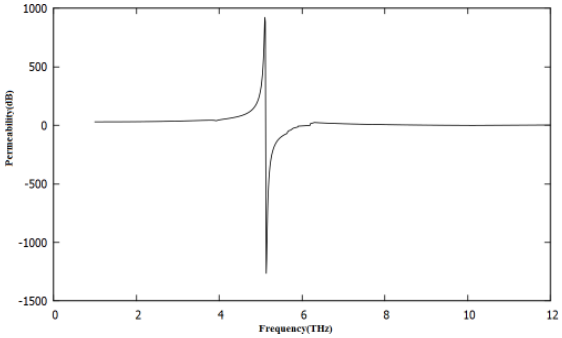

Fig. 8. Extracted relative permittivity and permeability of the proposed unit cell.

the magnetic field in a small circular region, the interaction of the toroid with the electromagnetic waves has been a subject of growing interest [23]. Due to the symmetry of the electromagnetic field, elements of toroidal symmetry rotate the polarization of light [24] and exhibit negative refraction [25]. The magnetic vortex structure has intrinsic orbital angular momentum and poloidal current density. Due to the superposition of the plane wave inside the vortex structure instead of rectilinear propagation, it follows the curvilinear trajectory [26]. The analysis of magnetic vortices as an array of concentric toroids was done using CST microwave studio simulation software. Since the ultrafast magnetic vortices excitation was found around THz frequency, the THz frequency electromagnetic field was used to excite the magnetic vortices.

The obtained results of the micromagnetic simulations are examined using ImageJ software, and exact geometrical parameters were found out. In this article, the electromagnetic properties of the array of toroids shown in Fig. 2 are numerically simulated via CST microwave studio. The dimension and the separation between the inclusion of the toroid are much smaller than the wavelength of electromagnetic radiation. The unit cell and the array of metamaterial structures are shown in Fig. 7. The unit cell of the structure consists of nine cobalt toroidal rings on the platinum substrate.

The proposed model was irradiated with the electromagnetic wave of frequency ranging from 0 to 12 THz. The proposed unit cell is simulated under perfect electric condition (PEC) and perfect magnetic condition (PMC) boundary condition. In this simulation, the scattering parameters retrieval method is used to obtain the effective anisotropic permeability tensor (μ) of the metamaterial.

The left-handed property was characterized by the reversal of the phase reflection and transmission coefficient at particular frequencies. The THz wave was made to pass through the proposed model to calculate the reflection (S_{11}) and transmission (S_{22}) parameters.

The permeability is calculated with reflection and transmission coefficient values. Fig. 8 depicts the real part of permeability. From the graph, it was observed that the real part of permeability value is positive till 5.12 THz, and after that, there is a strong dip in the permeability value and it becomes negative. The permeability value was found to be negative till 6.192 THz and it becomes positive.

In both the analysis method, the bandwidth is found to be almost 1 THz which is well suited for intriguing metamaterial applications such as giant optical chirality [27], wavefront control [28], and surface plasmon manipulation [29]. The main limitation of the proposed system lies in the narrow bandwidth range. Future directions are related to the improvement of bandwidth by considering more confined and tunable magnetization geometrical structures such as frustrated systems which include skyrmions [30], superconducting magnetic vortices [31], and antidot arrays [32].

VI. Conclusion

To conclude, we have proposed the toroidal magnetic metamaterial using an array of cobalt magnetic vortices as a spin-wave resonator. The analytical results depict that the FMR frequency depends on the damping factor and relaxation time. Numerical simulations using mumax[3] were performed to predict magnetization dynamics for varying magnetic fields. Using numerical simulation results, the Schloemann model was used to theoretically predict permeability as a function of frequency. The results depict that the permeability was negative in the vicinity of standing spin-wave resonance around 5.20–5.93 THz. The simulated cobalt magnetic vortices were successfully designed and simulated as a metamaterial toroidal unit cell using CST microwave studio, and scattering parameter retrieval method was used to find permeability as a function of frequency. In this case, the permeability was found to be negative in the frequency range from 5.125 to 6.192 THz. From this, we conclude that both methods show negative permeability almost in the same frequency range and this proposed magnetic metamaterial found to have negative refraction and possesses left-handed behavior in the same frequency range. According to our knowledge, it was the first demonstration of the magnetic toroidal response in metamaterials, which stimulated the progress of other metamaterials mimicking the toroidal topology. Therefore, a magnetic metamaterial specifically designed to maximize the toroidal component of an interaction with an external electromagnetic field may provide an outcome that can open up new possibilities for observation of toroidal left-handed response and its applications.

ACKNOWLEDGMENT

The work of Amuda Rajamani and Ponsudana Muthuraj was supported by DST SERB under Grant EMR/2016/00302, Government of India.

REFERENCES

[1] J. B. Pendry, A. J. Holden, D. J. Robbins, and W. J. Stewart, "Magnetism from conductors and enhanced nonlinear phenomena," *IEEE Trans. Microw. Theory Techn.*, vol. 47, no. 11, pp. 2075–2084, Nov. 1999, doi: 10.1109/22.798002.

[2] J. B. Pendry, "Controlling electromagnetic fields," *Science*, vol. 312, no. 5781, pp. 1780–1782, Jun. 2006, doi: 10.1126/science.1125907.

[3] K. Safa and P. Capper, *Springer Handbook of Electronic and Photonic Materials*, 2nd ed. Springer, 2017.

[4] K. Y. Guslienko, "Magnetic vortex state stability, reversal and dynamics in restricted geometries," *J. Nanoscience Nanotechnol.*, vol. 8, no. 6, pp. 2745–2760, Jun. 2008, doi: 10.1166/jnn.2008.003.

[5] R. V. Mikhaylovskiy, E. Hendry, and V. V. Kruglyak, "Negative permeability due to exchange spin-wave resonances in thin magnetic films with surface pinning," *Phys. Rev. B, Condens. Matter*, vol. 82, no. 19, Nov. 2010, doi: 10.1103/PhysRevB.82.195446.

[6] W. F. Brown, "Thermal fluctuations of a single-domain particle," *Phys. Rev.*, vol. 130, no. 5, pp. 1677–1686, Jun. 1963, doi: 10.1103/PhysRev.130.1677.

[7] D. Weller and M. F. Doerner, "Extremely high-density longitudinal magnetic recording media," *Annu. Rev. Mater. Sci.*, vol. 30, no. 1, pp. 611–644, Aug. 2000, doi: 10.1146/annurev.matsci.30.1.611.

[8] D. A. Gilbert *et al.*, "Realization of ground-state artificial skyrmion lattices at room temperature," *Nature Commun.*, vol. 6, no. 1, p. 8462, Dec. 2015, doi: 10.1038/ncomms9462.

[9] M.-Y. Im, K.-S. Lee, A. Vogel, J.-I. Hong, G. Meier, and P. Fischer, "Stochastic formation of magnetic vortex structures in asymmetric disks triggered by chaotic dynamics," *Nature Commun.*, vol. 5, no. 1, p. 5620, Dec. 2014, doi: 10.1038/ncomms6620.

[10] D. Polley, M. Pancaldi, M. Hudl, P. Vavassori, S. Urazhdin, and S. Bonetti, "THz-driven demagnetization with perpendicular magnetic anisotropy: Towards ultrafast ballistic switching," *J. Phys. D, Appl. Phys.*, vol. 51, no. 8, Feb. 2018, Art. no. 084001, doi: 10.1088/1361-6463/aaa863.

[11] M. Shalaby, C. Vicario, and C. P. Hauri, "Low frequency terahertz-induced demagnetization in ferromagnetic nickel," *Appl. Phys. Lett.*, vol. 108, no. 18, May 2016, Art. no. 182903, doi: 10.1063/1.4948472.

[12] M. Guyot and A. Globus, "Determination of the domain wall energy from initial magnetization curve in ferrimagnetic polycrystals," in *Proc. Amer. Inst. Phys. Conf.*, Jul. 2008, vol. 18, no. 1, p. 1382, doi: 10.1063/1.2947294.

[13] E. Schlömann, "Microwave behavior of partially magnetized ferrites," *J. Appl. Phys.*, vol. 41, no. 3, p. 1350, Mar. 1970, doi: 10.1063/1.1658936.

[14] Ü. Özgür, Y. Alivov, and H. Morkoç, "Microwave ferrites, part 1: Fundamental properties," *J. Mater. Sci., Mater. Electron.*, vol. 20, no. 9, pp. 789–834, 2009.

[15] G. T. Rado, "Theory of the microwave permeability tensor and Faraday effect in nonsaturated ferromagnetic materials," *Phys. Rev.*, vol. 89, no. 2, p. 529, Jan. 1953, doi: 10.1103/PhysRev.89.529.

[16] B. Ia Zel'Dovich, "Electromagnetic interaction with parity violation," *J. Exp. Theor. Phys.*, vol. 33, pp. 1531–1533, Dec. 1957.

[17] P. Tolédano *et al.*, "Primary ferrotoroidicity in antiferromagnets," *Phys. Rev. B, Condens. Matter*, vol. 92, no. 9, Sep. 2015, Art. no. 094431, doi: 10.1103/PhysRevB.92.094431.

[18] T. Kaelberer, V. A. Fedotov, N. Papasimakis, D. P. Tsai, and N. I. Zheludev, "Toroidal dipolar response in a metamaterial," *Science*, vol. 330, no. 6010, pp. 1510–1512, Dec. 2010, doi: 10.1126/science.1197172.

[19] D. G. Sannikov, "Phenomenological theory of the magnetoelectric effect in some boracites," *J. Exp. Theor. Phys.*, vol. 84, no. 2, pp. 293–299, Dec. 2010, doi: 10.1134/1.558116.

[20] N. Papasimakis, V. A. Fedotov, K. Marinov, and N. I. Zheludev, "Gyrotropy of a metamolecule: Wire on a torus," *Phys. Rev. Lett.*, vol. 103, no. 9, Aug. 2009, Art. no. 093901, doi: 10.1103/PhysRevLett.103.093901.

[21] K. Marinov, A. D. Boardman, V. A. Fedotov, and N. Zheludev, "Toroidal metamaterial," *New J. Phys.*, vol. 9, no. 9, p. 324, Sep. 2007, doi: 10.1088/1367-2630/9/9/324.

[22] J. Li *et al.*, "Optical responses of magnetic-vortex resonance in double-disk metamaterial variations," *Phys. Lett. A*, vol. 378, nos. 26–27, pp. 1871–1875, May 2014, doi: 10.1016/j.physleta.2014.04.049.

[23] N. A. Spaldin, M. Fiebig, and M. Mostovoy, "The toroidal moment in condensed-matter physics and its relation to the magnetoelectric effect," *J. Phys., Condens. Matter*, vol. 20, no. 43, Oct. 2008, Art. no. 434203, doi: 10.1088/0953-8984/20/43/434203.

[24] I. V. Stenishchev and A. A. Basharin, "Toroidal response in all-dielectric metamaterials based on water," *Sci. Rep.*, vol. 7, no. 1, Dec. 2017, Art. no. 9468, doi: 10.1038/s41598-017-07399-y.

[25] N. Papasimakis, V. A. Fedotov, V. Savinov, T. A. Raybould, and N. I. Zheludev, "Electromagnetic toroidal excitations in matter and free space," *Nature Mater.*, vol. 15, no. 3, pp. 263–271, Mar. 2016, doi: 10.1038/nmat4563.

[26] K. Y. Bliokh *et al.*, "Theory and applications of free-electron vortex states," *Phys. Rep.*, vol. 690, pp. 1–70, May 2017, doi: 10.1016/j.physrep.2017.05.006.

[27] B. Wang, J. Zhou, T. Koschny, M. Kafesaki, and C. M. Soukoulis, "Chiral metamaterials: Simulations and experiments," *J. Opt. A, Pure Appl. Opt.*, vol. 11, no. 11, Nov. 2009, Art. no. 114003, doi: 10.1088/1464-4258/11/11/114003.

[28] M. Kang, H.-T. Wang, and W. Zhu, "Wavefront manipulation with a dipolar metasurface under coherent control," *J. Appl. Phys.*, vol. 122, no. 1, Jul. 2017, Art. no. 013105, doi: 10.1063/1.4990996.

[29] Y. Liu, T. Zentgraf, G. Bartal, and X. Zhang, "Transformational plasmon optics," *Nano Lett.*, vol. 10, no. 6, pp. 1991–1997, Jun. 2010, doi: 10.1021/nl1008019.

[30] F. Ma, C. Reichhardt, W. Gan, C. J. O. Reichhardt, and W. S. Lew, "Emergent geometric frustration of artificial magnetic skyrmion crystals," *Phys. Rev. B, Condens. Matter*, vol. 94, no. 14, Oct. 2016, Art. no. 144405, doi: 10.1103/PhysRevB.94.144405.

[31] C. Reichhardt, C. J. Olson, and F. Nori, "Commensurate and incommensurate vortex states in superconductors with periodic pinning arrays," *Phys. Rev. B, Condens. Matter*, vol. 57, no. 13, pp. 7937–7943, Apr. 1998, doi: 10.1103/PhysRevB.57.7937.

[32] G. R. Berdiyorov, M. V. Milošević, and F. M. Peeters, "Novel commensurability effects in superconducting films with antidot arrays," *Phys. Rev. Lett.*, vol. 96, no. 20, May 2006, Art. no. 207001, doi: 10.1103/PhysRevLett.96.207001.

Madhumathi Rajaram received the master's and M.Phil. degrees from Bharathiar University, Coimbatore, India, in 2010 and 2012, respectively.

She is currently a Researcher with the Center for Nonlinear Dynamics, PSG College of Technology, Coimbatore. Her current research interest lies in magnetic metamaterials, magnetic vortices, magnetic skyrmions, and artificial frustrated systems.

Amuda Rajamani received the Ph.D. degree from the Centre for Nonlinear Dynamics, Bharathidasan University, Coimbatore, India, in 1997.

She is currently a Faculty Member with the Department of Physics and the Head of the Center for Nonlinear Dynamics, PSG College of Technology, Coimbatore. Her research interest includes nonlinear dynamics of magnetic systems and spintronics.

Dr. Rajamani completed two research projects funded by the University Grant Commission in 2005 and 2012 and one project funded by AICTE in 2010. She is currently the Principal Investigator of the project "investigation on the nonlinear dynamics of magnetic skyrmions" funded by DST-SERB, Government of India. She organized a one-month "5th SERB School on Nonlinear Dynamics" in 2016 funded by SERB, DST India. She organized a Lecture workshop on "Applications of Nonlinear Dynamics in Engineering and Technology" sponsored by INSA, IASc, and AScI, in 2009.

Ponsudana Muthuraj received the bachelor's degree in physics from the PSG College of Arts and Science, Coimbatore, India, in 2015, and the master's degree in physics from Government Arts College, Coimbatore, in 2017. She is currently pursuing the Ph.D. degree in the investigation of skyrmions in magnetic systems with the PSG College of Technology, Coimbatore.

She is currently a Project Assistant with the Centre for Nonlinear Dynamics, PSG College of Technology. Her research interests include magnetic skyrmions, skyrmionium, spin-transfer torque, and magnetic multilayers.

Brinda Arumugam received the Ph.D. degree from Anna University, Chennai, India, in 2016.

She is currently working as an Assistant Professor with the Department of Physics, PSG College of Technology, Coimbatore, India. Her research interests are non-linear dynamics, magnetic skyrmions, spin-valve pillars, metamaterials, and frustrated systems.

Kanimozhi Natarajan received the Ph.D. degree from Anna University, Chennai, India, in 2018.

She is currently working as an Assistant Professor with the Department of Physics, PSG College of Technology, Coimbatore, India. Her research interests are non-linear dynamics, spintronics, magnetic skyrmions, spin-valve pillars, and spin torque diodes.